The Journal of Chemical Physics

Accurate virial coefficients of gaseous krypton from state-of-the-art *ab initio* potential and polarizability of the krypton dimer

Cite as: J. Chem. Phys. **148**, 024306 (2018); https://doi.org/10.1063/1.5006970
Submitted: 29 September 2017 . Accepted: 22 December 2017 . Published Online: 11 January 2018

Bo Song, Jonathan M. Waldrop, Xiaopo Wang, and Konrad Patkowski

Accurate virial coefficients of gaseous krypton from state-of-the-art *ab initio* potential and polarizability of the krypton dimer

Bo Song,[1,a),b)] Jonathan M. Waldrop,[2,a)] Xiaopo Wang,[1] and Konrad Patkowski[2,c)]
[1]*Key Laboratory of Thermo-Fluid Science and Engineering, Ministry of Education, School of Energy and Power Engineering, Xi'an Jiaotong University, Xi'an, Shaanxi 710049, China*
[2]*Department of Chemistry and Biochemistry, Auburn University, Auburn, Alabama 36849, USA*

(Received 29 September 2017; accepted 22 December 2017; published online 11 January 2018)

We have developed a new krypton–krypton interaction-induced isotropic dipole polarizability curve based on high-level *ab initio* methods. The determination was carried out using the coupled-cluster singles and doubles plus perturbative triples method with very large basis sets up to augmented correlation-consistent sextuple zeta as well as the corrections for core-core and core-valence correlation and relativistic effects. The analytical function of polarizability and our recently constructed reference interatomic potential [J. M. Waldrop *et al.*, J. Chem. Phys. **142**, 204307 (2015)] were used to predict the thermophysical and electromagnetic properties of krypton gas. The second pressure, acoustic, and dielectric virial coefficients were computed for the temperature range of 116 K–5000 K using classical statistical mechanics supplemented with high-order quantum corrections. The virial coefficients calculated were compared with the generally less precise available experimental data as well as with values computed from other potentials in the literature {in particular, the recent highly accurate potential of Jäger *et al.* [J. Chem. Phys. **144**, 114304 (2016)]}. The detailed examination in this work suggests that the present theoretical prediction can be applied as reference values in disciplines involving thermophysical and electromagnetic properties of krypton gas. *Published by AIP Publishing.* https://doi.org/10.1063/1.5006970

I. INTRODUCTION

The macroscopic properties of fluids depend on the microscopic interactions between molecules and in principle they can be calculated from them.[1–4] In this way, with the help of modern computational techniques, it is now possible to obtain thermophysical properties of gases to high accuracy purely from theory.[5–12] This process involves two lengthy computations. At first, the potential energy curve $V(R)$, where R is the interatomic distance, is computed from first principles. Then, $V(R)$ is employed in expressions based on statistical mechanics and kinetic theory of dilute gases to yield thermophysical properties. The best known example is the theoretical results for helium[9] which have uncertainties that are significantly smaller (sometimes by nearly two orders of magnitude) than those of the corresponding measured quantities. Standard theoretical values of thermophysical properties are becoming important for two areas: instrument calibration[13–15] and metrology.[16–18] Other studies such as the development of thermodynamic and transport equations could also benefit from more accurate thermophysical data (e.g., Refs. 19–21).

We have recently constructed a new pair potential for krypton using coupled-cluster calculations up to the singles, doubles, triples, and perturbative quadruples level, including the corrections for core-core and core-valence correlation as well as relativistic effects.[10] Comparisons with the literature indicated that this potential is more accurate than any curve published previously. In this work, we have used the new potential together with classical statistical mechanics with quantum corrections to compute some thermophysical properties of krypton gas: the second pressure virial coefficient B and the second acoustic virial coefficient β_a for the range of 115.78 K (the triple-point temperature of naturally abundant krypton[22]) to 5000 K. The range of temperatures investigated is wide enough for most scientific and engineering purposes. In addition to thermophysical properties, the electromagnetic properties of simple gases are also valuable for pressure and temperature metrology.[23] For these reasons, we have also calculated the second dielectric virial coefficient B_ε of krypton using a semi-classical method for the same aforementioned temperature range. The calculations of B_ε require not only the pair potential but also the interaction-induced isotropic dipole polarizability $\Delta\alpha_{ave}(R)$ of the weakly bound dimer.

The rest of the article is structured as follows. We present in Sec. II the determination of the krypton–krypton interaction-induced polarizability as well as its analytical representation $\Delta\alpha_{ave}^{fit}(R)$ and the expressions for the lower- and upper-limits of its values. In Sec. III, our recent interatomic potential of the weakly bound krypton dimer[10] is briefly described for the sake of completeness. Section IV provides the detailed formulations for the computation of virial coefficients of krypton gas and the procedure to evaluate the uncertainty of theoretically calculated values. Section V contains a comparison of the experimental data and the values from some literature potentials with the present calculated values for the virial coefficients of krypton to assess carefully the performance of this work. It

[a)]B. Song and J. M. Waldrop contributed equally to this work.
[b)]E-mail: song.bo@xjtu.edu.cn
[c)]E-mail: patkowsk@auburn.edu

should be noted that, very recently, the Rostock group reported their fourth reference potential for pure noble gas molecules, namely, one for krypton,[12] following ones for helium,[6] neon,[7] and argon.[8] Jäger *et al.* used the best *ab initio* methods suitable for krypton to develop the potential energy curve for the two-body as well as the three-body interaction between krypton atoms. In Sec. V, considerable attention is paid to the agreement between the new *ab initio* potentials of Jäger *et al.*[12] and our work for the virial coefficients of krypton gas. Finally, we summarize in Sec. VI the main conclusions and give some perspectives of this work.

II. DEVELOPMENT OF INTERACTION-INDUCED POLARIZABILITY

The interaction-induced isotropic pair polarizability (the trace of the interaction-induced polarizability tensor) $\Delta\alpha_{\rm ave}(R)$ and its anisotropy $\Delta\alpha_{\rm aniso}(R)$ of the krypton dimer were calculated for the same interatomic distances as those used in the development of our high-accuracy Kr–Kr potential energy curve.[10] All calculations employed the counterpoise correction for the basis set superposition error.[24] Specifically, $\Delta\alpha_{\rm ave}(R)$ and $\Delta\alpha_{\rm aniso}(R)$ are defined by

$$\Delta\alpha_{\rm ave}(R) = \frac{1}{3}\left[\Delta\alpha_{\parallel}(R) + 2\Delta\alpha_{\perp}(R)\right], \tag{1}$$

$$\Delta\alpha_{\rm aniso}(R) = \left[\Delta\alpha_{\parallel}(R) - \Delta\alpha_{\perp}(R)\right], \tag{2}$$

$$\Delta\alpha_{\parallel}(R) = \alpha_{\parallel}^{\rm dimer}(R) - 2\alpha_{\parallel}^{\rm monomer}(R), \tag{3}$$

$$\Delta\alpha_{\perp}(R) = \alpha_{\perp}^{\rm dimer}(R) - 2\alpha_{\perp}^{\rm monomer}(R), \tag{4}$$

where $\alpha_{\parallel}^{\rm dimer}(R)$ and $\alpha_{\perp}^{\rm dimer}(R)$ are the components of the dimer polarizability that are parallel and perpendicular, respectively, to the internuclear axis at a given interatomic distance R and $\alpha_{\parallel}^{\rm monomer}(R)$ and $\alpha_{\perp}^{\rm monomer}(R)$ are the corresponding monomer components of polarizability calculated in the dimer basis.[8] All polarizabilities were calculated at the coupled-cluster singles and doubles plus perturbative triples [CCSD(T)] level and include corrections for core-core and core-valence correlation ($\Delta\alpha_{\rm ave}^{\rm AE-FC}$, $\Delta\alpha_{\rm aniso}^{\rm AE-FC}$) and relativistic effects ($\Delta\alpha_{\rm ave}^{\rm rel}$, $\Delta\alpha_{\rm aniso}^{\rm rel}$) so that

$$\Delta\alpha_{\rm ave} = \Delta\alpha_{\rm ave}^{\rm CCSD(T)/FC} + \Delta\alpha_{\rm ave}^{\rm AE-FC} + \Delta\alpha_{\rm ave}^{\rm rel}, \tag{5}$$

$$\Delta\alpha_{\rm aniso} = \Delta\alpha_{\rm aniso}^{\rm CCSD(T)/FC} + \Delta\alpha_{\rm aniso}^{\rm AE-FC} + \Delta\alpha_{\rm aniso}^{\rm rel}. \tag{6}$$

Calculations were performed using the CFOUR and MOLPRO codes.[25–27] Augmented correlation-consistent Dunning basis sets with X = D, T, Q, 5, 6 were used in all calculations: they included the polarized valence series,

TABLE I. Frozen-core CCSD(T) components of the interaction-induced pair polarizability and all-electron and relativistic corrections (a_0^3) for the krypton dimer near van der Waals minimum (R = 4.0 Å), computed in augmented Dunning basis sets aVXZ/aCVXZ/. . . as indicated.

	X =				
Component	D	T	Q	5	6
$\alpha_{\parallel}^{\rm CCSD(T)/FC}$/aV$X$Z	1.9897	2.5673	2.6037	2.6195	2.6246
$\alpha_{\perp}^{\rm CCSD(T)/FC}$/aV$X$Z	−0.9923	−1.2590	−1.2445	−1.2380	−1.2374
$\alpha_{\parallel}^{\rm CCSD(T)/FC}$/aCV$X$Z	2.0051	2.5805	2.6031	2.6192	
$\alpha_{\perp}^{\rm CCSD(T)/FC}$/aCV$X$Z	−0.9991	−1.2611	−1.2440	−1.2377	
$\alpha_{\parallel}^{\rm CCSD(T)/FC}$/awCV$X$Z	2.0440	2.5689	2.5998	2.6177	
$\alpha_{\perp}^{\rm CCSD(T)/FC}$/awCV$X$Z	−1.0144	−1.2564	−1.2421	−1.2369	
$\alpha_{\parallel}^{\rm AE-FC}$/aV$X$Z	−0.0030	−0.0183	−0.0246	−0.0410	
$\alpha_{\perp}^{\rm AE-FC}$/aV$X$Z	0.0015	0.0091	0.0121	0.0193	
$\alpha_{\parallel}^{\rm AE-FC}$/aCV$X$Z	−0.0077	−0.0357	−0.0472	−0.0559	
$\alpha_{\perp}^{\rm AE-FC}$/aCV$X$Z	0.0042	0.0185	0.0240	0.0277	
$\alpha_{\parallel}^{\rm AE-FC}$/awCV$X$Z	−0.0237	−0.0439	−0.0541	−0.0596	
$\alpha_{\perp}^{\rm AE-FC}$/awCV$X$Z	0.0120	0.0227	0.0272	0.0294	
$\alpha_{\parallel}^{\rm Rel}$/aV$X$Z	−0.0469	−0.0167	−0.0160	−0.0165	
$\alpha_{\perp}^{\rm Rel}$/aVXZ	0.0251	0.0128	0.0143	0.0127	
$\alpha_{\parallel}^{\rm Rel}$/aCV$X$Z	−0.0040	−0.0178	0.0066		
$\alpha_{\perp}^{\rm Rel}$/aCVXZ	0.0089	0.0137	0.0040		
$\alpha_{\parallel}^{\rm Rel}$/aCV$X$Z-DK	0.0237	0.0148	0.0117		
$\alpha_{\perp}^{\rm Rel}$/aCVXZ-DK	−0.0030	0.0007	0.0014		
$\alpha_{\parallel}^{\rm Rel}$/decontracted aV$X$Z	0.0185	0.0128	0.0103		
$\alpha_{\perp}^{\rm Rel}$/decontracted aVXZ	−0.0008	0.0015	0.0020		

aug-cc-pV*X*Z (aV*X*Z), polarized core and valence, aug-cc-pCV*X*Z (aCV*X*Z), weighted core-valence, aug-cc-pwCV*X*Z (awCV*X*Z), and aug-cc-pCV*X*Z recontracted for relativistic calculations, aug-cc-pCV*X*Z-DK (aCV*X*Z-DK).[12,28–32]

An initial assessment of the basis sets and corrections was performed on the same near van der Waals minimum distance as examined for the potential energy curve (R = 4.0 Å). The results of this examination can be seen in Table I. The uncertainty of a value in a particular basis is defined as the difference between that value and the corresponding result in the preceding basis. As such, the frozen-core results converge well in the aV6Z basis with values of 2.6246 ± 0.0051 a_0^3 in the parallel component and −1.2374 ± 0.0006 a_0^3 in the perpendicular component. Likewise, the core-core and core-valence correlation correction beyond the frozen-core approximation is reasonably well converged in the awCVQZ basis with values of −0.0541 ± 0.0102 and 0.0272 ± 0.0045 a_0^3 for the parallel and perpendicular components, respectively. It was determined that a basis set increase to awCV5Z was unnecessary given the minor improvement and the overall small size of the AE-FC correction. We have also checked if higher-order coupled-cluster excitations are important for the interaction-induced polarizability by performing a frozen-core CCSDT calculation in the aVDZ basis set (using the analytical implementation in CFOUR). At R = 4.0 Å, the difference between the CCSDT and CCSD(T) results is 0.0023 a_0^3 for the parallel component and −0.0003 a_0^3 for the perpendicular component. Thus, the full triples correction to the isotropic interaction-induced polarizability is just 0.0005 a_0^3 at this distance and we did not consider this correction any further.

The relativistic corrections were calculated analytically using the exact two-component (X2C) method.[33] This method is available in CFOUR,[34] though commented out in the public release due to the lack of picture change effects on the dipole moment operator. To validate the results obtained from the analytical code with a slightly incomplete treatment of relativity, we performed finite field calculations using the CFOUR and MOLPRO programs. The $\alpha_\parallel$ and $\alpha_\perp$ values for the monomer and dimer were calculated as numerical first derivatives of the analytical dipole moment (CFOUR) and second derivatives of the total energy (MOLPRO) with respect to a change in a uniform electric field. MOLPRO calculations of the relativistic effects used the second-order Douglas-Kroll-Hess (DKH) Hamiltonian, which provides an alternative to the X2C results.[35,36] As can be seen in Fig. 1, the numerical and analytical results from CFOUR agree extraordinarily well and the MOLPRO results provide satisfactory agreement given the difference in methods. As a side note, it was observed in the comparison of $\alpha_\parallel^{\text{dimer}}$ that the second-order DKH correction was around twice that of X2C, as shown in Fig. 2. This difference is small in absolute terms and cancels out in $\Delta\alpha_\parallel$ but is difficult to rationalize on its own. Due to the consistency between methods, the analytical approach was used to calculate the correction. The decontracted aV*X*Z results display the fastest basis set convergence, so we took the decontracted aVQZ values as the preferred ones, with values of 0.0103 ± 0.0025 a_0^3 for the parallel component and 0.0020 ± 0.0005 a_0^3 for the perpendicular component.

With the selection of the basis sets and levels of theory defined above, the interaction-induced isotropic pair polarizability $\Delta\alpha_{\text{ave}}$ at the near van der Waals minimum separation is 0.054 84 ± 0.002 97 a_0^3, where the uncertainty is the square root of the quadratic sum of the uncertainties of the contributing terms. This best level of theory was used to calculate $\Delta\alpha_{\text{ave}}(R)$ and $\Delta\alpha_{\text{aniso}}(R)$ at 25 values of R from 2.6 Å to 12.0 Å. The *ab initio* values for each term and the total $\Delta\alpha_{\text{ave}}$ can be found in Table II, while the corresponding results for $\Delta\alpha_{\text{aniso}}$ are presented in Table SI in the supplementary material. The near cancellation of $\Delta\alpha_\parallel$ and $\Delta\alpha_\perp$ results in values of $\Delta\alpha_{\text{ave}}$ very close to zero, as found previously for the argon dimer.[8]

Using a weighted least-squares routine,[37] the total $\Delta\alpha_{\text{ave}}$ and $\Delta\alpha_{\text{aniso}}$ were fitted to functions with forms[38–40]

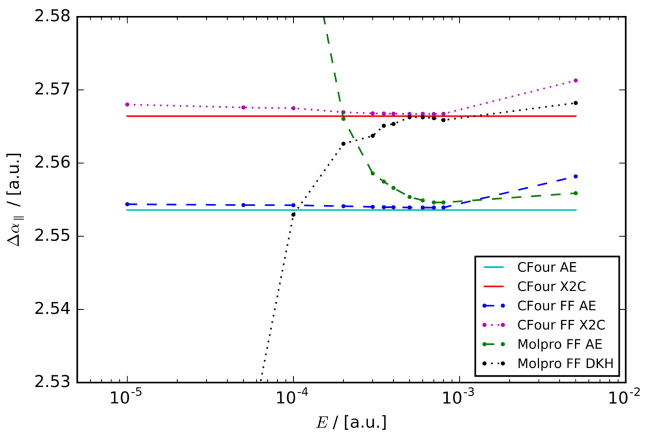

FIG. 1. The parallel component of the interaction-induced pair polarizability, $\Delta\alpha_\parallel$, as a function of electric field strength, E. AE denotes calculations including core-core and core-valence correlation and no relativistic correction. X2C and DKH denote calculations using the respective relativistic correction, while FF denotes calculations using a finite field method. All calculations for this test were performed in the decontracted aVTZ basis set.

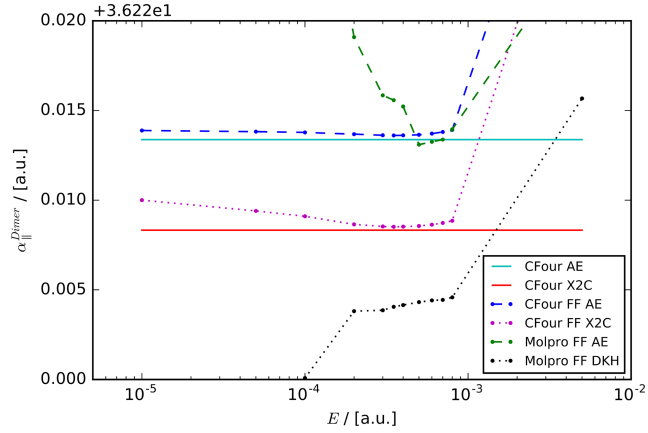

FIG. 2. The parallel component of the dimer polarizability, $\alpha_\parallel^{\text{Dimer}}$, as a function of electric field strength, E in atomic units. AE denotes calculations including core-core and core-valence correlation and no relativistic correction. X2C and DKH denote calculations using the respective relativistic correction, while FF denotes calculations using a finite field method. All calculations for this test were performed in the decontracted aVTZ basis set.

TABLE II. Contributions to the interaction-induced isotropic polarizability $\Delta\alpha_{\rm ave}$ for the krypton dimer, the total $\Delta\alpha_{\rm ave}$, and the total uncertainty $U(\Delta\alpha_{\rm ave})$ in units of a_0^3. The column $\Delta\alpha_{\rm ave}^{\rm fit}$ contains the values obtained from the fitted expression in Eq. (7).

R (Å)	$\Delta\alpha_{\rm ave}^{\rm CCSD(T)/FC}$	$\Delta\alpha_{\rm ave}^{\rm AE-FC}$	$\Delta\alpha_{\rm ave}^{\rm Rel}$	$\Delta\alpha_{\rm ave}$	$U(\Delta\alpha_{\rm ave})$	$\Delta\alpha_{\rm ave}^{\rm fit}$
2.60	−0.175 174 733	−0.020 902 900	−0.018 060 067	−0.214 137 700	0.013 476 933	−0.215 636 912
2.80	−0.312 638 567	−0.005 541 267	−0.000 928 067	−0.319 107 900	0.009 993 667	−0.315 336 594
3.00	−0.281 941 933	0.001 092 167	0.007 473 133	−0.273 376 633	0.008 011 233	−0.275 332 625
3.20	−0.194 681 200	0.003 224 533	0.010 414 167	−0.181 042 500	0.006 781 333	−0.183 014 852
3.40	−0.103 253 400	0.003 155 233	0.010 266 100	−0.089 832 067	0.005 577 233	−0.090 066 202
3.60	−0.029 548 700	0.002 200 600	0.008 675 167	−0.018 672 933	0.004 612 133	−0.017 982 438
3.70	−0.001 491 533	0.001 632 867	0.007 680 067	0.007 821 400	0.004 163 500	0.008 577 516
3.80	0.020 769 433	0.001 080 300	0.006 668 133	0.028 517 867	0.003 739 100	0.029 166 655
3.90	0.037 696 533	0.000 574 767	0.005 693 933	0.043 965 233	0.003 341 767	0.044 415 041
4.00	0.049 917 100	0.000 134 167	0.004 791 967	0.054 843 233	0.002 974 000	0.055 068 809
4.06	0.055 279 367	−0.000 095 467	0.004 293 867	0.059 477 767	0.002 767 800	0.059 576 680
4.10	0.058 127 900	−0.000 233 867	0.003 981 600	0.061 875 633	0.002 636 067	0.061 897 302
4.20	0.063 029 633	−0.000 528 767	0.003 270 300	0.065 771 167	0.002 330 267	0.065 634 625
4.30	0.065 282 433	−0.000 754 633	0.002 658 400	0.067 186 200	0.002 053 967	0.066 946 194
4.40	0.065 480 967	−0.000 918 767	0.002 140 600	0.066 702 800	0.001 806 900	0.066 412 705
4.60	0.061 698 800	−0.001 094 300	0.001 352 633	0.061 957 133	0.001 390 300	0.061 690 744
4.80	0.054 859 900	−0.001 122 400	0.000 829 033	0.054 566 533	0.001 061 133	0.054 412 776
5.00	0.047 011 267	−0.001 061 200	0.000 494 000	0.046 444 067	0.000 805 967	0.046 414 633
5.50	0.029 333 767	−0.000 764 333	0.000 120 933	0.028 690 367	0.000 426 233	0.028 796 038
6.00	0.017 528 567	−0.000 483 733	0.000 025 867	0.017 070 700	0.000 284 100	0.017 116 974
7.00	0.006 518 233	−0.000 181 367	0.000 002 433	0.006 339 300	0.000 160 700	0.006 311 046
8.00	0.002 761 167	−0.000 075 567	0.000 001 467	0.002 687 067	0.000 077 867	0.002 671 768
9.00	0.001 315 300	−0.000 035 533	0.000 000 733	0.001 280 500	0.000 039 433	0.001 277 486
10.00	0.000 684 067	−0.000 018 533	0.000 000 700	0.000 666 233	0.000 019 700	0.000 666 128
12.00	0.000 223 933	−0.000 006 100	0.000 000 233	0.000 218 067	0.000 006 067	0.000 217 420

$$\Delta\alpha_{\rm ave}^{\rm fit}(R) = \left(\frac{A^{\rm (ave)}}{R} + B^{\rm (ave)} + C^{\rm (ave)}R + D^{\rm (ave)}R^2\right) {\rm e}^{-\alpha^{\rm (ave)}R} + \sum\nolimits_{n=6,8} f_n\left(\beta^{\rm (ave)}R\right)\frac{C_n^{\rm (ave)}}{R^n}, \tag{7}$$

$$\Delta\alpha_{\rm aniso}^{\rm fit}(R) = \left(A^{\rm (aniso)}R + B^{\rm (aniso)}R^2\right) {\rm e}^{-\alpha^{\rm (aniso)}R} + \sum\nolimits_{n=3,6,8} f_n\left(\beta^{\rm (aniso)}R\right)\frac{C_n^{\rm (aniso)}}{R^n}, \tag{8}$$

where $f_n(x)$ is the Tang-Toennies damping function[41]

$$f_n(x) = 1 - {\rm e}^{-x}\sum\nolimits_{k=0}^{n}\frac{x^k}{k!}. \tag{9}$$

The weight for each *ab initio* point was the inverse square of the uncertainty and the fitted functions pass within the uncertainties of all calculated points. The $\Delta\alpha_{\rm ave}^{\rm fit}(R)$ function has MUE$\sigma = 0.140$ and $\Delta\alpha_{\rm aniso}^{\rm fit}(R)$ has MUE$\sigma = 0.216$, where the mean unsigned error with respect to uncertainty (MUEσ) is defined as

$${\rm MUE}\sigma = \frac{1}{N_R}\sum\nolimits_R \frac{|Fit(R) - Calc(R)|}{U(Calc(R))}. \tag{10}$$

In Eq. (10), $Fit(R)$ is either $\Delta\alpha_{\rm ave}^{\rm fit}(R)$ or $\Delta\alpha_{\rm aniso}^{\rm fit}(R)$ and $Calc(R)$ is the corresponding *ab initio* value. The long range C_n terms were fitted first to the data with $R \geq 8.0$ Å assuming no damping, then frozen throughout the rest of the procedure. The values of the fit parameters for $\Delta\alpha_{\rm ave}^{\rm fit}$ can be found in Table III; analogous parameters for the polarizability anisotropy are given in Table SII in the supplementary material.

Additionally, the upper- and lower-limit functions for both $\Delta\alpha_{\rm ave}^{\rm fit}(R)$ ($\Delta\alpha_{\rm ave}^{\rm fit,+}(R)$ and $\Delta\alpha_{\rm ave}^{\rm fit,-}(R)$) and $\Delta\alpha_{\rm aniso}^{\rm fit}(R)$

TABLE III. Parameters of the polarizability functions of $\Delta\alpha_{\rm ave}^{\rm fit}(R)$, $\Delta\alpha_{\rm ave}^{\rm fit,+}(R)$, and $\Delta\alpha_{\rm ave}^{\rm fit,-}(R)$ for the krypton dimer in Eq. (7).

Parameter	$\Delta\alpha_{\rm ave}^{\rm fit}(R)$	$\Delta\alpha_{\rm ave}^{\rm fit,+}(R)$	$\Delta\alpha_{\rm ave}^{\rm fit,-}(R)$	Units
$A^{\rm (ave)}$	−131 248.569 521	−144 967.965 213	−118 621.208 123	a_0^4
$B^{\rm (ave)}$	80 067.715 588	87 897.681 211	72 838.349 627	a_0^3
$C^{\rm (ave)}$	−15 649.670 075	−17 086.345 415	−14 319.251 185	a_0^2
$D^{\rm (ave)}$	958.404 374	1 040.655 286	882.044 335	a_0
$\alpha^{\rm (ave)}$	1.336 794	1.348 786	1.324 710	a_0^{-1}
$\beta^{\rm (ave)}$	0.857 610	0.867 624	0.845 646	a_0^{-1}
$C_6{}^{\rm (ave)}$	27 649.313 556 109 817	28 401.128 468 681 782	26 897.498 643 404 404	a_0^9
$C_8{}^{\rm (ave)}$	992 472.153 870 260 93	1 039 598.256 973 147 2	945 346.050 803 672 29	a_0^{11}

($\Delta\alpha^{\mathrm{fit},+}_{\mathrm{aniso}}(R)$ and $\Delta\alpha^{\mathrm{fit},-}_{\mathrm{aniso}}(R)$) were produced for the measurement of the uncertainty of the corresponding functions and the quantities derived from them. The functions $\Delta\alpha^{\mathrm{fit},+}_{\mathrm{ave}}(R)$ and $\Delta\alpha^{\mathrm{fit},-}_{\mathrm{ave}}(R)$ were fitted to $\Delta\alpha_{\mathrm{ave}} + U(\Delta\alpha_{\mathrm{ave}})$ and $\Delta\alpha_{\mathrm{ave}} - U(\Delta\alpha_{\mathrm{ave}})$, respectively, using the same functional form as $\Delta\alpha^{\mathrm{fit}}_{\mathrm{ave}}(R)$, and the equivalent procedure was used for the production of $\Delta\alpha^{\mathrm{fit},+}_{\mathrm{aniso}}(R)$ and $\Delta\alpha^{\mathrm{fit},-}_{\mathrm{aniso}}(R)$. The relation

$$\Delta\alpha^{\mathrm{fit},-}(R) < \Delta\alpha^{\mathrm{fit}}(R) < \Delta\alpha^{\mathrm{fit},+}(R) \tag{11}$$

is true for both quantities within the range of the fitted points but not necessarily outside of this range. The MUEσ values of the functions $\Delta\alpha^{\mathrm{fit},+}_{\mathrm{ave}}(R)$, $\Delta\alpha^{\mathrm{fit},-}_{\mathrm{ave}}(R)$, $\Delta\alpha^{\mathrm{fit},+}_{\mathrm{aniso}}(R)$, and $\Delta\alpha^{\mathrm{fit},-}_{\mathrm{aniso}}(R)$ are 0.163, 0.119, 0.212, and 0.222, respectively. The parameters for the upper- and lower-limit functions can be found in Table III for $\Delta\alpha^{\mathrm{fit}}_{\mathrm{ave}}$ and Table SII in the supplementary material for $\Delta\alpha^{\mathrm{fit}}_{\mathrm{aniso}}$.

III. POTENTIAL ENERGY CURVE

In our previous work,[10] we developed a new krypton–krypton interatomic potential based on high-level *ab initio* calculations. The analytic potential energy curve, used in this work in the same form, is given by

$$V(R) = \left(A + BR + \frac{C}{R}\right)e^{-\alpha R} - \sum_{n=3}^{4} f_{2n}(\beta R)\frac{C_{2n}}{R^{2n}}, \tag{12}$$

where $R \geq 1.8$ Å, A, B, C, α, β, C_6, and C_8 are the fit parameters and $f_{2n}(x)$ denote the Tang-Toennies damping functions,[41] Eq. (9). To avoid unphysical behavior at short distances ($R < 1.8$ Å), Eq. (12) is spliced continuously with a simpler expression

$$V(R) = \left(\frac{A_{\mathrm{sh}}}{R}\right)e^{-\alpha_{\mathrm{sh}}R+\beta_{\mathrm{sh}}R^2}. \tag{13}$$

In addition, we have constructed potentials $V^{+}(R)$ and $V^{-}(R)$ by fitting the same expression as $V(R)$ to $E + U(E)$ and $E - U(E)$, respectively. Here, the uncertainty $U(E)$ of the potential energy E was inferred by a careful examination of basis set convergence patterns.[10] The potential of Ref. 10 was computed within the Born-Oppenheimer approximation (which works extremely well for nuclei as heavy as krypton) and is exactly the same for all isotopologues of the krypton dimer. All fitted parameters in the analytical representations of $V(R)$, $V^{+}(R)$, and $V^{-}(R)$ are listed in Table IV.

TABLE IV. Parameters of the potential energy functions $V(R)$, $V^{+}(R)$, and $V^{-}(R)$ for the krypton dimer in Eqs. (12) and (13).

Parameter	$V(R)$	$V^{+}(R)$	$V^{-}(R)$	Unit
A	467.771 557	511.688	596.938	E_{h}
B	–43.111 875	–45.622	–56.519	$E_{\mathrm{h}} \cdot a_0^{-1}$
C	–509.601 417	–787.134	–997.849	$E_{\mathrm{h}} \cdot a_0$
α	1.566 575	1.558	1.572	a_0^{-1}
β	4.083 794	1.832	1.285	a_0^{-1}
C_6	126.790 499	126.498	127.083	$E_{\mathrm{h}} \cdot a_0^{6}$
C_8	5268.109 217	5096.285	5439.933	$E_{\mathrm{h}} \cdot a_0^{8}$
A_{sh}	1296.0	1296.0	1296.0	$E_{\mathrm{h}} \cdot a_0$
α_{sh}	3.067 950	2.744	2.900	a_0^{-1}
β_{sh}	0.324 0714	0.239	0.280	a_0^{-2}

IV. THEORETICAL EVALUATION OF VIRIAL COEFFICIENTS

In this section, we calculate the second pressure, acoustic, and dielectric virial coefficients and estimate their uncertainties.

A. Second pressure virial coefficient

We employ the classical statistical-mechanics formulas with second-order or third-order quantum corrections to compute the virial coefficients of krypton. The calculations of the second pressure virial coefficient B by statistical mechanics have been studied extensively and the explicit expressions are presented in a large number of scientific publications (for example, in Ref. 42). For the convenience of the reader, we still list the details of the formulations necessary to compute B up to the third-order quantum corrections,

$$B = B_{\mathrm{cl}} + \lambda B_{\mathrm{qm},1} + \lambda^2 B_{\mathrm{qm},2} + \lambda^3 B_{\mathrm{qm},3}, \tag{14}$$

where $\lambda = \hbar^2\beta/12m$, $\hbar = h/2\pi$, and $\beta = 1/k_B T$. m is the relative molecular mass (83.798 for krypton in this work), h is the Planck constant, k_{B} is the Boltzmann constant,[43] and T is the temperature. In the case of a completely isotropic potential $V(R)$ (no angular dependence), the classical and quantum contributions can be written as follows:

$$B_{\mathrm{cl}} = -2\pi N_{\mathrm{A}}\int_0^{\infty}\left[\exp(-\beta V) - 1\right]R^2 dR, \tag{15}$$

$$B_{\mathrm{qm},1} = 2\pi N_{\mathrm{A}}\int_0^{\infty}(\beta V')^2\exp(-\beta V)\,R^2 dR, \tag{16}$$

$$B_{\mathrm{qm},2} = -2\pi N_{\mathrm{A}}\int_0^{\infty}\left[\frac{6}{5}(\beta V'')^2 + \frac{12}{5R^2}(\beta V')^2 + \frac{4}{3R}(\beta V')^3 - \frac{1}{6}(\beta V')^4\right]\exp(-\beta V)\,R^2 dR, \tag{17}$$

$$B_{\mathrm{qm},3} = 2\pi N_{\mathrm{A}}\int_0^{\infty}\left[\frac{36}{35}(\beta V''')^2 + \frac{216}{35R^2}(\beta V'')^2 + \frac{24}{21}(\beta V'')^3 + \frac{24}{5R}(\beta V')(\beta V'')^2 + \frac{288}{315R^3}(\beta V')^3 - \frac{6}{5}(\beta V')^2(\beta V'')^2 - \frac{2}{15R^2}(\beta V')^4 - \frac{2}{5R}(\beta V')^5 + \frac{1}{30}(\beta V')^6\right]\exp(-\beta V)\,R^2 dR, \tag{18}$$

in which N_A denotes the Avogadro constant and $V' = dV/dR$, $V'' = d^2V/dR^2$, and $V''' = d^3V/dR^3$.

B. Second acoustic virial coefficient

The expressions for the second acoustic virial coefficient β_a are related to those for the second pressure virial coefficient B and its first and second temperature derivatives B' and B''. The semi-classical expansion of the second acoustic virial coefficient in powers of λ is[8]

$$\beta_a = \beta_{a,cl} + \lambda\beta_{a,qm,1} + \lambda^2\beta_{a,qm,2}, \tag{19}$$

where the individual terms are formulated as

$$\beta_{a,cl} = 4\pi N_A \int_0^\infty \left[1 - \exp(-\beta V)\left(1 + \frac{2}{5}\beta V + \frac{2}{15}(\beta V)^2\right)\right] R^2 dR, \tag{20}$$

$$\beta_{a,qm,1} = 4\pi N_A \int_0^\infty \left[\frac{3}{5} - \frac{2}{5}\beta V + \frac{2}{15}(\beta V)^2\right] (\beta V')^2 \exp(-\beta V)\, R^2 dR, \tag{21}$$

$$\begin{aligned}\beta_{a,qm,2} = 4\pi N_A \int_0^\infty \Bigg\{ &\left[-\frac{6}{5}(\beta V'')^2 - \frac{12}{5R^2}(\beta V')^2 - \frac{20}{9R}(\beta V')^3 + \frac{13}{30}(\beta V')^4\right] \\ &+ \left[\frac{4}{5}(\beta V'')^2 + \frac{8}{5R^2}(\beta V')^2 + \frac{56}{45R}(\beta V')^3 - \frac{1}{5}(\beta V')^4\right]\beta V \\ &+ \left[-\frac{4}{25}(\beta V'')^2 - \frac{8}{25R^2}(\beta V')^2 - \frac{8}{45R}(\beta V')^3 + \frac{1}{45}(\beta V')^4\right](\beta V)^2\Bigg\} \exp(-\beta V)\, R^2 dR.\end{aligned} \tag{22}$$

C. Second dielectric virial coefficient

The formulas for the dielectric virial coefficients can be derived from the expansion of the Clausius-Mossotti function. The second dielectric virial coefficient can again be approximated as the sum of a classical term and of quantum corrections up to second order[40]

$$B_\varepsilon = B_{\varepsilon,cl} + \lambda B_{\varepsilon,qm,1} + \lambda^2 B_{\varepsilon,qm,2}, \tag{23}$$

where

$$B_{\varepsilon,cl} = \frac{8\pi^2 N_A^2}{3} \int_0^\infty \Delta\alpha_{ave} \exp(-\beta V)\, R^2 dR, \tag{24}$$

$$\begin{aligned}B_{\varepsilon,qm,1} = -\frac{8\pi^2 N_A^2}{3} \int_0^\infty &\left[\Delta\alpha_{ave}(\beta V')^2 - 2\Delta\alpha'_{ave}\beta V'\right] \\ &\times \exp(-\beta V)\, R^2 dR,\end{aligned} \tag{25}$$

$$B_{\varepsilon,qm,2} = \frac{16\pi^2 N_A^2}{5} \int_0^\infty (\Delta\alpha_{ave} f + g) \exp(-\beta V)\, R^2 dR, \tag{26}$$

$$f = (\beta V'')^2 + \frac{2}{R^2}(\beta V')^2 + \frac{10}{9R}(\beta V')^3 - \frac{5}{36}(\beta V')^4, \tag{27}$$

$$\begin{aligned}g = \Delta\alpha'_{ave}\left[-\frac{4}{R^2}\beta V' - \frac{10}{3R}(\beta V')^2 + \frac{5}{9}(\beta V')^3\right] \\ - 2\Delta\alpha''_{ave}\beta V''.\end{aligned} \tag{28}$$

Here,

$$\Delta\alpha'_{ave} = d\Delta\alpha_{ave}/dR, \tag{29}$$

$$\Delta\alpha''_{ave} = d^2\Delta\alpha_{ave}/dR^2. \tag{30}$$

D. Uncertainty

There are several possible sources of uncertainty in the present calculation. First, quantum effects become important at low temperatures depending on the molecule in question. The lower-limit temperature for the calculations considered in this work is 115.78 K, the triple-point temperature of krypton. At this temperature, the corresponding ratio of the thermal de Broglie wavelength to the atomic diameter is much smaller than one, i.e., $\left(h/\sqrt{2\pi m k_B T}\right)/\sigma = 0.05 \ll 1$. This guarantees that we can use classical statistical-mechanics formulae with second-order or third-order quantum corrections to compute the different virials of krypton for the whole temperature range.

In addition, Moszynski *et al.*[44] suggested that the use of Padé approximants could better represent full quantum-mechanical results at lower temperatures. Our earlier unpublished work on the second dielectric virial coefficient of neon at 116 K showed that the Padé approximant of order [1/1] reproduced the semi-classical value up to five digits of precision. This agreement further justifies the correctness of classical treatments supplemented by quantum expansions in powers of λ.

The other major contribution to the uncertainty of our calculated values is attributed to the uncertainty of the potential and polarizability of the krypton dimer. As mentioned above, we generated $V^+(R)$, $V^-(R)$, $\Delta\alpha_{ave}^{fit,+}(R)$, and $\Delta\alpha_{ave}^{fit,-}(R)$ expressions that account for the corresponding lower- and upper-limit ranges of potential energies and interaction-induced polarizabilities. Following the work of Hurly *et al.*,[45,46] we attempted to estimate the uncertainty U of the present theoretical results in the following manner:

$$U(X) = \frac{|X_{V^+} - X_{V^-}|}{2}, \tag{31}$$

where X denotes virial coefficients calculated from V^+ and V^-. The calculation of Cencek *et al.*[38] suggested that the influence of the uncertainties in $V(R)$ on the values of B_ε was negligible. Hence, for the second dielectric virial coefficient, the uncertainty of the theoretical values was estimated as

$$U(B_\varepsilon) = \frac{\left| B_{\varepsilon,\Delta\alpha_{ave}^{fit,+}} - B_{\varepsilon,\Delta\alpha_{ave}^{fit,-}} \right|}{2}. \quad (32)$$

V. COMPARISON WITH VIRIAL COEFFICIENT VALUES FROM THE LITERATURE

Here we compare the results of our calculations with values published elsewhere for the second pressure, acoustic, and dielectric virial coefficients.

A. Second pressure virial coefficient

Very recently, Jäger *et al.*[12] reported the calculation of the second pressure virial coefficient of krypton from their new potential. Figure 3 of the present article illustrates that the *ab initio* pressure virial values of Jäger *et al.* are perfectly consistent with our theoretical values over a wide temperature range. The difference between the two *ab initio* values decreases from 1 $cm^3 \cdot mol^{-1}$ at 150 K down to 0.3 $cm^3 \cdot mol^{-1}$ at room temperature and further down to below 0.1 $cm^3 \cdot mol^{-1}$ above 2000 K. Figure 3 also shows the uncertainty of our calculated values, which was evaluated from the potentials $V^+(R)$ and $V^-(R)$ by the procedure discussed above. It is clear that the differences between the second virial coefficient of Jäger *et al.* and the results of this work never exceed the theoretically estimated uncertainty for the complete temperature range.

There is a large number of experimental data for the second virial coefficient of krypton, published more than 30 years ago. The information on the sources of literature was summarized in the compilation of Dymond *et al.*[47] It should be noted that an experimental determination of a strictly two-body quantity such as $B(T)$ requires caution to eliminate three- and higher-body effects even at low densities of the gas.[48] In their Fig. 1, Jäger *et al.*[12] compared their computed values with measured data sets for the second pressure virial coefficient. Because of the excellent agreement between the values of Jäger *et al.* and this work, the same pattern could be drawn for the comparison of the experimental data with our computed values. In many cases, a deviation of more than ±1 $cm^3 \cdot mol^{-1}$ could be observed between the theory and measurements for the second pressure virial coefficient, the maximum deviation being −16 $cm^3 \cdot mol^{-1}$ at the low temperature of 120 K. Aziz and Slaman[49] did not consider the second pressure virial coefficient of krypton as primary data in the development of their empirical potentials due to the inconsistency of experimental data, which is partly supported by the rather large disagreements in Fig. 1 of Jäger *et al.*[12] Moreover, considering the fact that the uncertainty of theoretical values for krypton is normally lower than that of the experimental data,[47] we conclude that both the present results and those of Jäger *et al.* may be employed as recommended values for the second pressure virial coefficient of this gas.

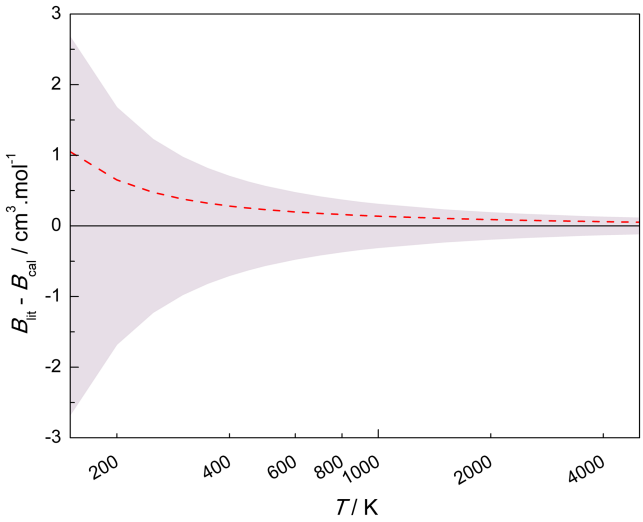

FIG. 3. Absolute deviations of the literature second pressure virial coefficient data, B_{lit}, from the values calculated in this work, B_{cal}, for krypton as a function of temperature. Data sources: (red dashed line) calculated from the potential by Jäger *et al.*[12] The shaded area corresponds to the uncertainty of B_{cal}.

B. Second acoustic virial coefficient

To the best of our knowledge, only one publication with measurements of the second acoustic virial coefficient of krypton is to be found in the literature. Ewing *et al.*[50] built a cylindrical interferometer to measure the speed of sound of gases. Values of the second acoustic virial coefficient of krypton were reported for 285 K, 305 K, and 320 K, with a reported standard uncertainty of around ±1 $cm^3 \cdot mol^{-1}$. Figure 4 shows that the experimental data of Ewing *et al.* are in close agreement of ±(0.5–1.0) $cm^3 \cdot mol^{-1}$ with the theoretically calculated values of this work.

Figure 4 also presents the differences between values computed in this work and those from several krypton potentials in the literature, namely, the well-recognized empirical potential of Dham *et al.*,[51] the old *ab initio* potential of Slavíček *et al.*,[52] and the new, high-accuracy potential of Jäger *et al.*[12] The second acoustic virial coefficient from the potential of Dham *et al.* agrees with the theoretically calculated values of this work at $T \leq 500$ K. However, the absolute deviation begins to exceed the estimated uncertainty of our theoretical values at higher temperatures. The computed values from the

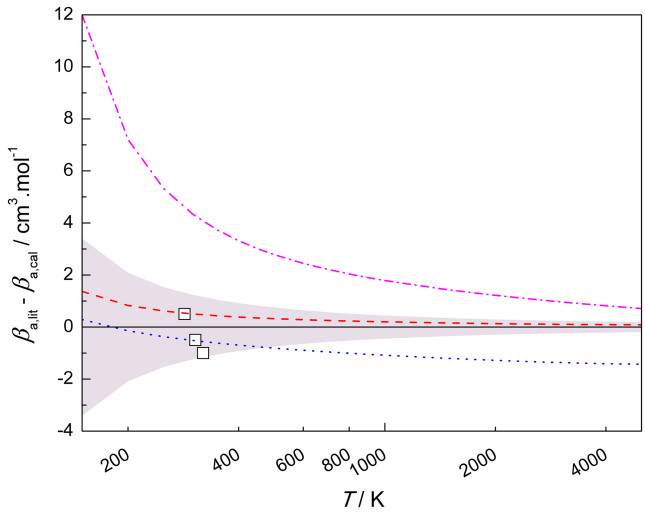

FIG. 4. Absolute deviations of the literature second acoustic virial coefficient data, $\beta_{a,lit}$, from the values calculated in this work, $\beta_{a,cal}$, for krypton as a function of temperature. Data sources: (black open squares) Ewing *et al.*;[50] (blue dotted line) calculated from the potential by Dham *et al.*;[51] (magenta dot line) calculated from the potential by Slavíček *et al.*;[52] (red dashed line) calculated from the potential by Jäger *et al.*[12] The shaded area corresponds to the uncertainty of $\beta_{a,cal}$.

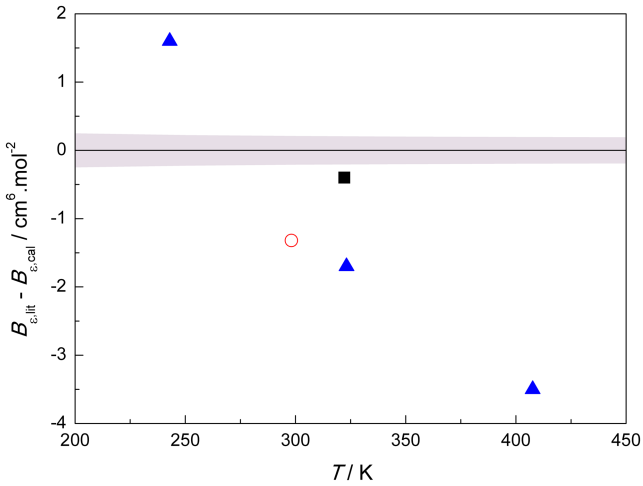

FIG. 5. Absolute deviations of the literature second dielectric virial coefficient data, $B_{\varepsilon,\mathrm{lit}}$, from the values calculated in this work, $B_{\varepsilon,\mathrm{cal}}$, for krypton as a function of temperature. Data sources: (black filled square) Orcutt and Cole;[53] (red open circle) Vidal and Lallemand;[54] (blue filled triangles) Huot and Bose.[55] The shaded area corresponds to the uncertainty of $B_{\varepsilon,\mathrm{cal}}$.

potential of Slavíček *et al.* exhibit a relatively large disagreement with those of this work: the differences are larger than the corresponding uncertainties of our theoretical values over the whole temperature range. On the other hand, one can see in Fig. 4 that there is good agreement for the second acoustic virial coefficient between the new *ab initio* potential of Jäger *et al.* and that of this work. The absolute difference lies within the uncertainty range of our theoretical calculation for temperatures up to 5000 K. We suggest that the present computed values can be used with confidence in different fields wherever values of the second acoustic virial coefficient of krypton are required.

C. Second dielectric virial coefficient

Three sets of experimental data are available in the literature for the second dielectric virial coefficient of krypton.[53–55] Figure 5 shows a comparison of the experimental data with the values calculated here. Orcutt and Cole[53] reported one data point at ambient temperature, where the difference slightly exceeds our theoretical uncertainty. The data point by Vidal and Lallemand[54] at 25 °C shows a disagreement of −1.3 cm^6·mol^{-2}, which is six times larger than the estimated uncertainty of our calculated value. A larger scatter of ±(2–4) cm^6·mol^{-2} can be observed for the deviation of the data by Huot and Bose[55] with respect to the values calculated here. The inconsistency of measurements from different laboratories implies that the prediction of this work may be applied as reference values for the second dielectric virial coefficient.

TABLE V. Virial coefficients of krypton and their estimated uncertainties as a function of temperature. The temperatures 115.78 K and 209.48 K correspond, respectively, to the triple- and critical-point temperatures of krypton. The virial coefficient values at other temperatures are available upon request for the range between 115.78 K and 5000 K.

T (K)	B (cm^3 · mol^{-1})	$U(B)$ (cm^3 · mol^{-1})	β_a (cm^3 · mol^{-1})	$U(\beta_a)$ (cm^3 · mol^{-1})	B_ε (cm^6 · mol^{-2})	$U(B_\varepsilon)$ (cm^6 · mol^{-2})
115.78	−321.30	4.44	−347.47	6.11	10.923	0.384
150	−198.04	2.68	−191.03	3.39	8.7080	0.2976
200	−116.34	1.68	−94.934	2.071	7.2778	0.2447
209.48	−106.55	1.57	−83.747	1.934	7.1080	0.2386
250	−75.164	1.23	−48.270	1.52	6.5637	0.2199
273.15	−62.372	1.09	−33.980	1.37	6.3408	0.2125
273.16	−62.368	1.09	−33.975	1.37	6.3407	0.2125
293.15	−53.306	1.00	−23.911	1.26	6.1817	0.2075
298.15	−51.271	0.98	−21.658	1.23	6.1458	0.2064
300	−50.539	0.98	−20.848	1.22	6.1329	0.2060
350	−34.244	0.82	−2.9210	1.0372	5.8418	0.1973
400	−22.716	0.71	9.6263	0.9079	5.6296	0.1916
450	−14.164	0.62	18.835	0.813	5.4663	0.1876
500	−7.5918	0.56	25.832	0.740	5.3354	0.1847
600	1.7896	0.47	35.644	0.635	5.1354	0.1810
700	8.1039	0.41	42.069	0.561	4.9861	0.1789
800	12.596	0.37	46.498	0.507	4.8676	0.1778
900	15.922	0.34	49.663	0.466	4.7693	0.1772
1000	18.459	0.31	51.983	0.433	4.6851	0.1770
1500	25.184	0.23	57.344	0.333	4.3807	0.1784
2000	27.779	0.19	58.588	0.282	4.1717	0.1811
2500	28.906	0.17	58.517	0.250	4.0089	0.1839
3000	29.382	0.15	57.940	0.228	3.8745	0.1867
3500	29.528	0.14	57.157	0.212	3.7600	0.1894
4000	29.495	0.13	56.297	0.201	3.6604	0.1919
4500	29.360	0.12	55.419	0.191	3.5726	0.1943
5000	29.166	0.11	54.551	0.184	3.4945	0.1965

VI. CONCLUSIONS

We have developed a new interaction-induced isotropic polarizability for the krypton dimer and used it together with our recent interaction potential to calculate the second pressure, acoustic, and dielectric virial coefficients of krypton gas. The coupled-cluster method at the CCSD(T) level as well as basis sets up to aV6Z was selected to determine the interaction-induced isotropic polarizability $\Delta\alpha_{\rm ave}(R)$. The corrections for core-core correlation, core-valence correlation, and relativistic effects were also included to improve the quality of $\Delta\alpha_{\rm ave}(R)$. As a result, values of the interaction-induced isotropic polarizability were determined with low uncertainty for the krypton dimer at 25 different interatomic distances R covering the range of 2.6–12.0 Å. An analytical expression of $\Delta\alpha_{\rm ave}^{\rm fit}(R)$ was obtained by fitting the individual values in order to facilitate the calculation of the second dielectric virial coefficient.

Using the newly developed interaction-induced polarizability, together with our highly accurate interatomic potential,[10] we computed the second pressure, acoustic, and dielectric virial coefficients of krypton gas. Calculations were performed using classical statistical mechanics supplemented with quantum corrections up to second or third orders. The theoretically calculated values of virial coefficients are listed in Table V for the temperature range of 115.78 K–5000 K. The corresponding uncertainty given in Table V is estimated from the difference between the values calculated using $V^{+}(R)$, $V^{-}(R)$, $\Delta\alpha_{\rm ave}^{\rm fit+}(R)$, and $\Delta\alpha_{\rm ave}^{\rm fit-}(R)$.

Comparisons of the literature data were performed with the values computed in this work. Some inconsistencies were found with respect to the relatively small number of experimental data. On the other hand, the two new *ab initio* potentials, the one of Jäger *et al.*[12] and the one of this work, exhibit excellent agreement for the calculations of the second pressure and acoustic virial coefficients. All things considered, we believe that the present theoretically predicted values can be used as reference values for the different virial coefficients of krypton gas. Given the scarcity of reliable experimental data, accurate measurements of thermophysical and electromagnetic properties of krypton gas are desirable to further check the validity of the present predictions.

SUPPLEMENTARY MATERIAL

See supplementary material for the results of the interaction-induced anisotropy polarizability of the krypton dimer.

ACKNOWLEDGMENTS

The authors thank Dr. Mark Plimmer, of the Conservatoire National des Arts et Métiers, for his kind reading of the manuscript. We also thank Dr. Lan Cheng, of the Johns Hopkins University, for his help with the X2C calculations. This work was supported by the National Key R&D Program of China (Grant No. 2016YFE0204200), the U.S. National Science Foundation CAREER Award No. CHE-1351978, and the 111 Project (No. B16038).

[1] J. O. Hirschfelder, C. F. Curtiss, and R. B. Bird, *Molecular Theory of Gases and Liquids* (Wiley, New York, 1954).
[2] S. Chapman and T. G. Cowling, *The Mathematical Theory of Non-Uniform Gases: An Account of the Kinetic Theory of Viscosity, Thermal Conduction and Diffusion of Gases* (Cambridge University Press, Cambridge, 1970).
[3] G. C. Maitland, M. Rigby, E. B. Smith, and W. A. Wakeham, *Intermolecular Forces: Their Origin and Determination* (Clarendon Press, Oxford, 1981).
[4] F. R. W. McCourt, J. J. M. Beenakker, W. E. Köhler, and I. Kuščer, *Non-Equilibrium Phenomena in Polyatomic Gases* (Clarendon Press, Oxford, 1990).
[5] R. Hellmann, "Thermophysical properties of industrially relevant fluids and fluid mixtures from pure theory," in *19th European Conference on Thermophysical Properties* (Aristotle University of Thessaloniki, Greece, Thessaloniki, 2011).
[6] E. Bich, R. Hellmann, and E. Vogel, Mol. Phys. **105**, 3035–3049 (2007).
[7] E. Bich, R. Hellmann, and E. Vogel, Mol. Phys. **106**, 813–825 (2008); **106**, 1107–1122 (2008).
[8] E. Vogel, B. Jäger, R. Hellmann, and E. Bich, Mol. Phys. **108**, 3335–3352 (2010).
[9] W. Cencek, M. Przybytek, J. Komasa, J. B. Mehl, B. Jeziorski, and K. Szalewicz, J. Chem. Phys. **136**, 224303 (2012).
[10] J. M. Waldrop, B. Song, K. Patkowski, and X. Wang, J. Chem. Phys. **142**, 204307 (2015).
[11] B. Song, X. Wang, and Z. Liu, Mol. Simul. **42**, 9–13 (2016).
[12] B. Jäger, R. Hellmann, E. Bich, and E. Vogel, J. Chem. Phys. **144**, 114304 (2016).
[13] R. F. Berg and M. R. Moldover, J. Phys. Chem. Ref. Data **41**, 043104 (2012).
[14] D. Seibt, S. Herrmann, E. Vogel, E. Bich, and E. Hassel, J. Chem. Eng. Data **54**, 2626–2637 (2009).
[15] M. Schäfer, M. Richter, and R. Span, J. Chem. Thermodyn. **89**, 7–15 (2015).
[16] R. M. Gavioso, D. M. Ripa, P. P. M. Steur, C. Gaiser, T. Zandt, B. Fellmuth, M. de Podesta, R. Underwood, G. Sutton, L. Pitre, F. Sparasci, L. Risegari, L. Gianfrani, A. Castrillo, and G. Machin, Philos. Trans. R. Soc., A **374**, 20150046 (2016).
[17] C. Gaiser, B. Fellmuth, and T. Zandt, Int. J. Thermophys. **35**, 395–404 (2014).
[18] R. M. Gavioso, D. M. Ripa, P. P. M. Steur, C. Gaiser, D. Truong, C. Guianvarc'h, P. Tarizzo, F. M. Stuart, and R. Dematteis, Metrologia **52**, S274–S304 (2015).
[19] M. J. Assael, J. A. Assael, M. L. Huber, R. A. Perkins, and Y. Takata, J. Phys. Chem. Ref. Data **40**, 033101 (2011).
[20] B. Jäger, R. Hellmann, E. Bich, and E. Vogel, J. Chem. Phys. **135**, 084308 (2011).
[21] K. R. Shaul, A. J. Schultz, D. A. Kofke, and M. R. Moldover, Chem. Phys. Lett. **531**, 11–17 (2012).
[22] K. D. Hill, AIP Conf. Proc. **1552**, 198–203 (2013).
[23] J. W. Schmidt, R. M. Gavioso, E. F. May, and M. R. Moldover, Phys. Rev. Lett. **98**, 254504 (2007).
[24] S. Boys and F. Bernardi, Mol. Phys. **19**, 553–566 (1970).
[25] J. F. Stanton, J. Gauss, M. E. Harding, P. G. Szalay, A. A. Auer, R. J. Bartlett, U. Benedikt, C. Berger, D. E. Bernholdt, Y. J. Bomble, O. Christiansen, M. Heckert, O. Heun, C. Huber, T.-C. Jagau, D. Jonsson, J. Jusélius, K. Klein, W. J. Lauderdale, D. A. Matthews, T. Metzroth, D. P. O'Neill, D. R. Price, E. Prochnow, K. Ruud, F. Schiffmann, S. Stopkowicz, A. Tajti, J. Vázquez, F. Wang, and J. D. Watts, CFOUR, a quantum chemical program package, containing the integral packages MOLECULE (J. Almlöf and P. R. Taylor), PROPS (P. R. Taylor), ABACUS (T. Helgaker, H. J. Aa. Jensen, P. Jørgensen, and J. Olsen), and ECP routines by A. V. Mitin and C. van Wüllen. For the current version, see http://www.cfour.de.
[26] H.-J. Werner, P. J. Knowles, G. Knizia, F. R. Manby, and M. Schütz, Wiley Interdiscip. Rev.: Comput. Mol. Sci. **2**, 242–253 (2012).
[27] H.-J. Werner, P. J. Knowles, G. Knizia, F. R. Manby, M. Schütz, P. Celani, W. Györffy, D. Kats, T. Korona, R. Lindh, A. Mitrushenkov, G. Rauhut, K. R. Shamasundar, T. B. Adler, R. D. Amos, A. Bernhardsson, A. Berning, D. L. Cooper, M. J. O. Deegan, A. J. Dobbyn, F. Eckert, E. Goll, C. Hampel, A. Hesselmann, G. Hetzer, T. Hrenar, G. Jansen, C. Köppl, Y. Liu, A. W. Lloyd, R. A. Mata, A. J. May, S. J. McNicholas, W. Meyer, M. E. Mura, A. Nicklaß, D. P. O'Neill, P. Palmieri, D. Peng, K. Pflüger, R. Pitzer, M. Reiher, T. Shiozaki, H. Stoll, A. J. Stone, R. Tarroni, T. Thorsteinsson, and M. Wang, MOLPRO, version 2012.1, a package of *ab initio* programs, 2012, see http://www.molpro.net.

[28]T. H. Dunning, Jr., J. Chem. Phys. **90**, 1007 (1989).
[29]R. A. Kendall, T. H. Dunning, Jr., and R. J. Harrison, J. Chem. Phys. **96**, 6796 (1992).
[30]A. K. Wilson, D. E. Woon, K. A. Peterson, and T. H. Dunning, Jr., J. Chem. Phys. **110**, 7667 (1999).
[31]N. B. Balabanov and K. A. Peterson, J. Chem. Phys. **123**, 064107 (2005).
[32]N. J. DeYonker, K. A. Peterson, and A. K. Wilson, J. Phys. Chem. A **111**, 11383–11393 (2007).
[33]K. G. Dyall, J. Chem. Phys. **115**, 9136 (2001).
[34]L. Cheng, S. Stopkowicz, and J. Gauss, Int. J. Quantum Chem. **114**, 1108–1127 (2014).
[35]M. Douglas and N. M. Kroll, Ann. Phys. **82**, 89–155 (1974).
[36]B. A. Hess, Phys. Rev. A **33**, 3742 (1986).
[37]E. Jones, T. Oliphant, P. Peterson *et al.*, SciPy: Open Source Scientific Tools for Python, 2001, http://www.scipy.org/ (Online, accessed September 22, 2017).
[38]W. Cencek, J. Komasa, and K. Szalewicz, J. Chem. Phys. **135**, 014301 (2011).
[39]C. Hättig, H. Larsen, J. Olsen, P. Jørgensen, H. Koch, B. Fernández, and A. Rizzo, J. Chem. Phys. **111**, 10099 (1999).
[40]R. Moszynski, T. G. A. Heijmen, P. E. S. Wormer, and A. van der Avoird, J. Chem. Phys. **104**, 6997 (1996).
[41]K. T. Tang and J. P. Toennies, J. Chem. Phys. **80**, 3726 (1984).
[42]M. E. Boyd, S. Y. Larsen, and J. E. Kilpatrick, J. Chem. Phys. **50**, 4034 (1969).
[43]P. J. Mohr, D. B. Newell, and B. N. Taylor, J. Phys. Chem. Ref. Data **45**, 043102 (2016).
[44]R. Moszynski, T. G. A. Heijmen, and A. van der Avoird, Chem. Phys. Lett. **247**, 440–446 (1995).
[45]J. J. Hurly and M. R. Moldover, J. Res. Natl. Inst. Stand. Technol. **105**, 667–688 (2000).
[46]J. J. Hurly and J. B. Mehl, J. Res. Natl. Inst. Stand. Technol. **112**, 75–94 (2007).
[47]J. H. Dymond, R. C. Wilhoit, K. N. Marsh, K. C. Wong, and M. Frenkel, in *Landolt-Börnstein: Numerical Data and Functional Relationships in Science and Technology: New Series, Group IV: Physical Chemistry*, edited by M. Frenkel and K. N. Marsh (Springer, New York, 2002), Vol. 21A, Chap. 2, pp. 64–67.
[48]J. Wiebke, E. Pahl, and P. Schwerdtfeger, J. Chem. Phys. **137**, 064702 (2012).
[49]R. A. Aziz and M. J. Slaman, Chem. Eng. Commun. **78**, 153–165 (1989).
[50]M. B. Ewing, M. L. McGlashan, and J. P. M. Trusler, J. Chem. Thermodyn. **17**, 549–559 (1985).
[51]A. K. Dham, A. R. Allnatt, W. J. Meath, and R. A. Aziz, Mol. Phys. **67**, 1291–1307 (1989).
[52]P. Slavíček, R. Kalus, P. Paška, I. Odvárková, P. Hobza, and A. Malijevský, J. Chem. Phys. **119**, 2102 (2003).
[53]R. H. Orcutt and R. H. Cole, J. Chem. Phys. **46**, 697 (1967).
[54]D. Vidal and M. Lallemand, J. Chem. Phys. **64**, 4293 (1976).
[55]J. Huot and T. K. Bose, J. Chem. Phys. **95**, 2683 (1991).